Atmos. Chem. Phys. Discuss., 13, 2835–2876, 2013
www.atmos-chem-phys-discuss.net/13/2835/2013/
doi:10.5194/acpd-13-2835-2013

Atmospheric Chemistry and Physics Discussions

Ozone and fine particle in the western Yangtze River Delta: an overview of 1-yr data at the SORPES station

A. J. Ding[1], C. B. Fu[1], X. Q. Yang[1], J. N. Sun[1], L. F. Zheng[1], Y. N. Xie[1], E. Herrmann[1,2], T. Petäjä[2], V.-M. Kerminen[2], and M. Kulmala[2]

[1]Institute for Climate and Global Change Research & School of Atmospheric Sciences, Nanjing University, Nanjing, 210093, China
[2] Department of Physics, University of Helsinki, 00014 Helsinki, Finland

Received: 8 January 2013 – Accepted: 13 January 2013 – Published: 28 January 2013

Correspondence to: A. J. Ding (dingaj@nju.edu.cn)

Published by Copernicus Publications on behalf of the European Geosciences Union.

Abstract

This work presents an overview of 1-yr measurements of ozone (O_3) and fine particular matter ($PM_{2.5}$) and related trace gases at a recently developed regional background site, the Station for Observing Regional Processes of the Earth System (SORPES), in the western part of the Yangtze River Delta (YRD) in East China. O_3 and $PM_{2.5}$ showed distinguished seasonal cycles but with contrast patterns: O_3 reached a maximum in warm seasons but $PM_{2.5}$ in cold seasons. Correlation analysis suggests a VOC-sensitive regime for O_3 chemistry and also indicates a substantial formation of secondary aerosols under conditions of high O_3 in summer. Compared with the National Ambient Air Quality Standards in China, our measurements report 15 days of O_3 exceedance and 148 days of $PM_{2.5}$ exceedance during the 1-yr period, suggesting a severe air pollution situation in this region. Case studies for typical O_3 and $PM_{2.5}$ episodes demonstrated that these episodes were generally associated with an air mass transport pathway over the mid-YRD, i.e. along the Nanjing-Shanghai axis with its city clusters, and showed that synoptic weather played an important role in air pollution, especially for O_3. Agricultural burning activities caused high $PM_{2.5}$ and O_3 pollution during harvest seasons, especially in June. A calculation of potential source contributions based on Lagrangian dispersion simulations suggests that emissions from the YRD contributed to over 70 % of the O_3 precursor CO, with a majority from the middle-YRD. North-YRD and the North China Plain are the main contributors to $PM_{2.5}$ pollution in this region, especially for the burning episode days. This work shows an important environmental impact from industrialization and urbanization in the YRD region, and suggests an urgent need for improving air quality in these areas through collaborative control measures among different administrative regions.

ACPD
13, 2835–2876, 2013

1 Introduction

Ozone (O_3) and fine particular matter ($PM_{2.5}$) are two of the most important components in the tropospheric atmosphere because of their effects on human health, biosphere and climate (e.g. Chameides et al. 1999a, b; Jerrett et al., 2009; Allen et al., 2012). Because of complex sources and chemical reactions, and a relatively long atmospheric lifetime in the atmosphere that favor regional/long-range transport, both pollutants are of great concern for regional air quality but are all very difficult to control (Cooper et al., 2005; Zhang et al., 2008; van Donkelaar et al., 2010).

Due to huge consumption of fossil fuels in the past decades (Richter et al., 2005), many regions in China have been experiencing heavy and even increasing O_3 and $PM_{2.5}$ pollution, especially in the developed coastal regions, such as the Beijing-Tianjin Area, Pearl River Delta (PRD) and Yangtze River Delta (YRD) (Ding et al., 2008; Xu et al., 2008; Wang et al., 2009; Tie and Cao, 2009). In the latest decades, a large number of studies were performed to address their spatio-temporal distributions and to understand their causes in those developed regions. A relatively long history of research and hence a good understanding have been gained in the Beijing-Tianjin and the PRD regions (e.g. Zhang et al., 2003; Wang et al., 2003, 2006, 2009, 2010; Lin et al., 2008), while in the YRD region, in which only few measurement studies have been conducted, large knowledge gaps still exist in the understanding of the characteristics and main sources of O_3 and $PM_{2.5}$.

The YRD region is located in the east part of the Eastern China Plain adjacent to the most polluted North China Plain (Fig. 1b). It includes the mega-city Shanghai and the well-industrialized and urbanized areas of the southern part of Jiangsu Province and the northern part of Zhejiang Province, with over ten mega/large cities, such as Hangzhou, Suzhou, Wuxi and Changzhou lying along the middle-YRD, i.e. the Shanghai-Nanjing axis (see Fig. 1c). Consisting of only 2 percent of the land area, this region produces over 20 percent of China's Gross Domestic Product (GDP), making it the most densely populated region in the country and one of its emission hotspots.

ACPD
13, 2835–2876, 2013

Furthermore, this area and the surrounding Eastern China Plain also form one of the most important agricultural bases in China with wheat and rice planted alternatively in cold and warm seasons. Previous studies suggested that both O_3 and aerosols could affect the crop growth in this region (e.g. Feng et al., 2003; Chameidies, 1999a, b), and also suggest that agricultural activities, such as fertilization and intensive straw burning activities, could significantly influence regional air quality in this region (e.g. Ye et al., 2011, Wang et al. 2004, 2009; Ding et al., 2013b). In addition, the YRD is located in a typical monsoon region, with warm and humid conditions in summer and cold and dry weather in winter. The complex monsoon and synoptic weather may play an important role in air pollution transport and formation in this region. Therefore, this is a region of great interest to study the complex interactions between human activities, biosphere and the atmosphere.

The earliest measurement study of O_3 in the YRD region started in 1990s at the Lin'an site, a regional GAW station located in the southeast YRD (Luo et al., 2000; Wang et al., 2001). Studies at this site provided the first picture of the seasonal behaviors of O_3 and its precursors in the southeast YRD (Wang et al., 2001, 2004; Xu et al., 2008). Besides Lin'an, there were only very limited studies of O_3 made in urban sites in some YRD cities (e.g. Tu et al., 2007; Geng et al., 2008; Ran et al., 2012). $PM_{2.5}$ measurements in this region have been performed only in recent years (e.g. Fu et al. 2008; Zhou et al. 2009; Li et al., 2011; Huang et al., 2012; Zhang et al., 2013). However, most of these studies were done close to Shanghai, i.e. the eastern YRD, and mainly cover short periods of time. For the more inland western YRD area, which is generally downwind from the entire YRD under prevailing winds between northeast and southeast, only very few studies of O_3 and $PM_{2.5}$ were conducted, and these only at urban sites (e.g. Wang et al., 2002; Yang et al., 2005; Tu et al., 2007). Therefore there is a significant lack of knowledge on the regional characteristics of these pollutants, which is inherently important for the assessment of the regional impacts of the YRD emissions on atmospheric composition and also for the policy making of air pollution measures in west YRD cities like Nanjing.

ACPD
13, 2835–2876, 2013

To fill the knowledge gap, continuous online measurements of trace gases, aerosols and other relevant parameters were carried out at a background site SORPES (Station for Observing Regional Processes of the Earth System), an integrated measurement platform for the study of atmospheric environment and climate change. This work presents the first results of 1-yr measurements of O_3 and $PM_{2.5}$ and related trace gases at the site during August 2011–July 2012, and gives a synthesis analysis about their characteristics and causes by using Lagrangian dispersion modeling. We give detailed descriptions about the measurement site and instruments and an introduction of general meteorological conditions in Sect. 2, and present main results, including overall temporal variation, correlation analysis and case studies in Sect. 3. A summary is given in Sect. 4.

2 Description of experiment and meteorological conditions

2.1 Brief introduction to the SORPES site

The Station for Observing Regional Processes of the Earth System is a research and experiment platform developed by the Institute for Climate and Global Change Research (ICGCR) at Nanjing University (NJU) in collaboration with the University of Helsinki. The overall objective of this platform is to characterize the temporal variation of key parameters related to climate change and to understand the interactions of different regional processes of the Earth System in East China, a region strongly influenced by monsoon weather and by intensive human activities. With a joint effort between NJU and the University of Helsinki, SORPES is in the process of being developed into a SMEAR (Station for Measuring Ecosystem-Atmosphere Relations) type measurement station (Hari et al., 2009), but focuses more on the impact of human activities on the climate and on the environment system in the rapidly urbanized and industrialized Yangtze River Delta region. Considering the geography, climate, and the environment characteristics in East China, measurements at the SORPES sites

ACPD
13, 2835–2876, 2013

focus on four major processes: land-surface processes, air pollution-climate interaction, ecosystem-atmosphere interaction, and hydrology and water cycle. The entire platform will be developed to an integrated observation network with a "flagship" central site, few "satellite" sites and mobile platforms in the vicinity.

At the current stage, the efforts mainly focus on the development of the "flagship" central site which is located on the Xianlin Campus of NJU in the suburban area northeast of Nanjing (118°57′10″E, 32°07′14″N), about 20 km from the downtown area (Fig. 1a). Since the prevailing winds in this region are from northeast and southeast in the cold and warm seasons, respectively, the Xianlin site is generally upwind from downtown Nanjing and can be considered as a regional background station for atmospheric chemistry studies. As Nanjing is located in the northwest of the YRD region (Fig. 1c), the site is also generally downwind of the most developed middle-YRD regions including the megacity Shanghai and the Suzhou-Wuxi-Changzhou city cluster. Therefore, the measurements at the station can help address impacts from these areas of highly intensive human activity in a regional air quality perspective.

Measurements of trace gases, aerosols, and relevant meteorological parameters began from summer 2011. Most of the instruments of trace gases and aerosol concentrations are housed on the top floor of a laboratory building, which sits on the top of a hill about 40 m above the surrounding landscape. Trace gases like O_3, carbon monoxide (CO), sulfur dioxide (SO_2), Nitric oxide (NO), total reactive nitrogen (NO_y) and $PM_{2.5}$ mass were routinely measured. O_3, SO_2, NO, NO_y and CO trace gases were measured with a resolution of 1 min using online analyzers (Thermo Instruments, TEI 49i, 43i, 42i, 42CY and 48i, respectively), and those instruments were weekly span calibrated and daily zero checked. $PM_{2.5}$ mass concentrations were measured using a mass analyzer (SHARP-5030). For the 1-yr period (August 2011–July 2012), these instruments performed well and data coverage of most of the species were higher than 95 %. Besides $PM_{2.5}$ mass, aerosol size distribution measurement were also available since November 2011 by using an Air Ion Spectrometer (AIS) and Different Mobility Particle Sizer (DMPS), and those data will be reported in a separate paper (Herrmann et al., 2013).

ACPD
13, 2835–2876, 2013

2.2 Meteorological conditions and transport features

Monthly averaged general meteorological parameters at Nanjing are shown in Table 1. It suggests that the region had a contrast air temperature in winter and summer, with monthly means from about 3 °C in January to 29.4 °C in July. High relative humidity (RH) and a large amount of rainfall occurred in August (290 mm in total), and less precipitation and low RH appeared in autumn and winter. Wind data suggest that the prevailing wind was from northeast in winter and from east and southeast in summer (see wind-rose shown on Fig. 1a).

To further understand the general transport characteristics of air masses recorded at the site, we conducted 7-day backward particle release simulations using a Lagrangian dispersion model Hybrid Single-Particle Lagrangian Integrated Trajectory (HYSPLIT) model, developed in the Air Resource Laboratory of the National Oceanic and Atmospheric Administration (Draxler and Hess, 1998). In this study, we applied the model following a method developed by Ding et al. (2013a). Briefly, for each hour during the study period, the model was run 7-day backwardly with 3000 particles released at 100 m a.g.l. over the site. The spatiotemporal distributions of these particles were used to further calculate the source-receptor relationship. The residence time of particles at 100 m level was used to identify "footprint" retroplume and to calculate the potential source contribution (PSC) by using an emission inventory. This method has been evaluated and has shown very good performance in the simulation if long-living species like CO, and shows wide application in understanding the transport and origins of air pollutants (Stohl et al., 2003; Cooper et al., 2005; Ding et al., 2009). In this study, 3-h high resolution (0.5 degree by 0.5 degree) Global Data Assimilation System (GDAS) data were used to drive the model. A high resolution emission inventory (0.2 by 0.2 degree), developed by Zhang et al. (2009) was used to calculate the PSC of CO and $PM_{2.5}$.

Based on a 7-day backward particle release simulation for each hour during the 1-yr study period, Fig. 2a–d give the averaged distribution of retroplumes at the site for spring, summer, autumn, and winter, respectively. These figures give clear pictures

ACPD
13, 2835–2876, 2013

about the transport history of air masses recorded at the site. Previous studies suggested that Asian monsoon dominates the regional/long-range transport of the air pollution in East Asia (e.g. Liu et al., 2002; Naja and Akimoto, 2004). In summer and winter, the retroplumes show completely different transport patterns under the influence of the Asian monsoon (Fig. 2b and d). In summer, the air masses were generally originating from the Northwest Pacific Ocean and the South China Sea and were transported to the site by southeasterly/southwesterly summer monsoon. But during winter time, the air masses were generally originating from the inner Eurasian Continent and transported southeasterly by the winter monsoon, resulting in a high residence time from Mongolia to the North China Plain. Associated with a continental high pressure system, those continental air masses in winter were generally transported to the site from the Yellow Sea in the northeast of the site by clockwise anti-cyclone flows. Spring and autumn are the two transition periods with air masses mainly transported in the eastern China and the adjacent oceans. As we show in Sect. 3.1, the distinguished transport patterns in different seasons controlled the seasonal behaviors of primary pollutants at the site. The transport patterns also indicate that the observed air masses could carry information from the entire eastern part of China and further suggest that the SORPES site is an ideal regional background station and will be useful to assess the change of the atmosphere on a large scale.

3 Results and discussions

3.1 Seasonal behaviors

With 1-yr continuous measurements for the period of August 2011–July 2012, we got the first picture of seasonal behaviors of O_3, $PM_{2.5}$, and relevant precursors in the west YRD region. Figures 3a–f give monthly variation of O_3, $PM_{2.5}$, SO_2, CO, NO_y, and NO, respectively.

ACPD
13, 2835–2876, 2013

Ozone shows a distinguished seasonal pattern, with an overall broad O_3 peak in the summer and early autumn (a maximum in July and a secondary maximum in September) and a minimum in November. The observed seasonal behavior of O_3 at the site is fairly different from what has been reported in any other places in China. For instance, a summer minimum and autumn maximum of O_3 were recorded at Hong Kong in South China (Wang et al., 2009), an early summer (June) broad maximum of O_3 were reported in Beijing (Ding et al., 2008; Lin et al., 2008). For the YRD region, available observations from either surface measurement at Lin'an (Xu et al., 2008) or satellite retrievals at Shanghai (Dufour et al., 2010) suggest a later spring (May) maximum and early autumn (September) secondary maximum, which was attributed to a well-defined summertime decease of O_3 associated with "clean" maritime air transported from the Pacific Ocean by the monsoons. Considering the geographical location of Nanjing, which is downwind of the YRD under the influence of southeasterly summer monsoon, the emissions in the YRD region might be the main cause for a substantial O_3 formation in summer, resulting in a different seasonal cycle of O_3 compared to other coastal sites in the East/Southeast YRD. In fact, the CO and NO_y data (Figs. 3d–f) shows that these precursors were still on fairly high levels (about 600 ppbv and 25 ppbv, respectively) in summer.

For the fine particle $PM_{2.5}$, Fig. 3b shows an overall well-defined seasonal pattern with a maximum in autumn (November) and a minimum in summer (July). This clear seasonal pattern could be due to the change of emission and deposition processes. Emission of particulate matter is generally high in cold seasons because heating in the northern China needs more consumption of fossil fuels (Zhang et al., 2009) and windblown dusts are also higher under the dry weather and strong wind in winter. Deposition should also have a strong seasonal variation because high precipitation (Table 1) favors wet-deposition and high soil humidity and the growth of deciduous plants may enhance the dry deposition of particular matter in warm seasons (Zhang et al., 2001). $PM_{2.5}$ mass concentration also showed strong month-to-month variations, e.g. a sharp peak in June and a drop in February. The June peak was mainly associated

ACPD
13, 2835–2876, 2013

with intensive activities of straw burning as we discuss in Sect. 3. The drop of $PM_{2.5}$ concentration together with other primary pollutants, such as SO_2, CO and NO_y, in February is attributed mainly to the winter break of the Chinese Spring Festival, which started from the end of January.

Other primary trace gases all show dramatic seasonal cycles but also some unique month-to-month variation patterns. For instance, NO_y concentration increased after the autumn with a maximum appearing in December, which seems to be mainly caused by the increase of directly emitted NO. High NO concentrations also cause titration of O_3 in November and December (Fig. 3a). SO_2 concentration shows a strong increase in winter but a significant drop in November. The drop was associated with the $PM_{2.5}$ maximum and a relatively high RH (Fig. 3b and Table 1), suggesting a possible role of heterogeneous reactions (Ravishankara, 1997). In fact, in this region a high frequency of fogs generally occurs in autumn, especially in November.

3.2 Inter-species correlations

Investigation of correlations of different species will help interpret the data and gain some insights into the related mechanisms/processes. In Fig. 4a–d, we give scatter plots of O_3-NO_y, SO_2-NO_y, CO-NO_y and $PM_{2.5}$-O_3, respectively. To differentiate the correlations under the influence of relevant meteorological/environmental factors, the data points are color-coded with different parameters (e.g. air temperature, relative humidity and O_3 mixing ratio).

Figure 4a shows that O_3 measured at the site has an overall negative correlation with NO_y. The color of data points shows that the negative correlation mainly exists for data of low air temperature, suggesting a titration effect of freshly emitted NO with O_3 in cold seasons and during night. In contrast, a pronounced positive correlation between O_3-NO_y prevailed during high air temperature, which mainly appeared in daytime of warm seasons with a moderate level (< 100 ppbv) of NO_y. These results suggest a strong photochemical production of O_3 in this region in summer, resulting in the seasonal cycle pattern of O_3 shown in Fig. 3a.

ACPD
13, 2835–2876, 2013

The two primary pollutants SO_2 and NO_y show a quite good correlation (Fig. 4b). However, their ratio is much lower than that previous reported at Lin'an ten years ago (e.g. Wang et al., 2004). This can be explained by a significant reduction of SO_2 emission from power plants but an increased NO_x emission associated with a huge consumption of petroleum fuels in the past decade in this region (Richter et al., 2005; Zhang et al., 2009). The color of data points given in Fig. 4b shows an obvious relationship between RH and SO_2/NO_y ratio. A better correlation and a higher SO_2/NO_y ratio is obtained for air with low humidity, while for the humid air masses the relationship is much more scattered, and the ratio of SO_2/NO_y is obviously low, suggesting a higher conversion of SO_2 to sulfate and/or deposition in the humid environment (Khoder, 2002).

A scatter plot of CO-NO_y given in Fig.4c is color-coded with O_3 concentration. It's very interesting to see that high O_3 are generally associated with air masses of high CO/NO_y ratio. For NO_y lower than 100 ppbv, an increase of CO always results in higher O_3 concentration, but NOy reverses. As volatile organic compounds (VOCs) generally have good correlation with CO and play a similar role as CO in the photochemical ozone production (Atkinson, 2000), the O_3-CO-NO_y relationship strongly indicates a VOCs-limited regime of O_3 formation in this region. Geng et al. (2008) also reported a VOCs-limited regime in Shanghai by using measured and modeling results. It needs to be pointed out that recent years controlling of NO_x has been put forward in China, however, our results suggest that an inappropriate control of NO_x alone may lead to increased O_3 pollution for the YRD region.

Figure 4d gives a scatter-plot of $PM_{2.5}$ and O_3, the two most important pollutants, color-coded with air temperature. Interestingly, a negative correlation can be found for low air temperature samples but a pronounced positive correlation existed for high temperature data points. The anti-correlation for cold air could be mainly attributed to the titration effect of high NO concentration, which was associated with high primary $PM_{2.5}$ in cold seasons, and the positive correlation with an increasing slope (see the polynomial fitting for samples with air temperature over 30 °C) indicates a substantial

ACPD
13, 2835–2876, 2013

formation of secondary fine particles in summer associated with high concentration of O_3. Here the secondary particle formation may be related to high conversion rate of SO_2 to sulfate under a high concentration of oxidants (Khoder, 2002), and/or be related to formation of secondary organic aerosols with high O_3 concentrations (Kamens et al., 1999) because biogenic emission of VOCs could also be high in the upwind rural area under a condition of high air temperature and solar radiation in summer. The measurements of aerosol size distribution at the SORPES site also show strong new particle formation at the site under a condition of high O_3 levels (Herrmann et al., 2013). Previous studies of $PM_{2.5}$ chemical compositions in Shanghai and Nanjing (e.g. Wang et al., 2002, 2006) and an intensive measurement of water soluble ions at the SORPES station (Ding et al., 2013b) all suggested that sulfate was the most dominate ion in $PM_{2.5}$. The detailed mechanisms still need to be further addressed by long-term measurement of aerosol chemical composition.

3.3 Discussions on O_3 and $PM_{2.5}$ episodes

3.3.1 Overall statistics of exceedances to standards

The above analysis has shown overall high O_3 concentrations in summer and high $PM_{2.5}$ levels during the entire year, with extremely high $PM_{2.5}$ concentration in the cold seasons. To further understand the air pollution situation, Table 2 gives statistical information of O_3 and $PM_{2.5}$ mass concentrations with a comparison to the Ambient Air Quality Standards in China (AAQS-CN), which were released in early 2012 by the China State Council but will be implemented nation-wide in 2016 (MEP, 2012). During the 1-yr period, there were 15 days of O_3 exceedances in total, with most of them occurred in warm seasons (July–October). This frequency is higher than that observed in Shanghai by Ran et al., (2012). For $PM_{2.5}$, the annual averaged concentration is 75.6 $\mu g\,m^{-3}$, more than twice of the annual standard (35 $\mu g\,m^{-3}$), and 148 days (40 % of the year, mainly in cold seasons from September to June) exceeded the daily limit of 75 $\mu g\,m^{-3}$. It is noteworthy that the annual mean $PM_{2.5}$ concentration is almost equal to

ACPD
13, 2835–2876, 2013

the estimation given by van Donkelaar et al. (2010), which suggested a multi-year average of $PM_{2.5}$ mass concentration over 80 µg m^{-3} in East China by using satellite data during 2001–2006. As our measurements were conducted in upwind from Nanjing, the results show a severe regional air quality problem in the YRD.

To help understand the causes of O_3 episodes, we give the diurnal patterns of O_3, $PM_{2.5}$ and related species for the 15 days with O_3 exceedances, together with those for 1-day before and after those exceedances, as well as the annual means in Fig. 5. O_3 shows a typical diurnal cycle with a minimum in the early morning and the daily maximum in the early afternoon (~ 14:00 LT). But during the episode days, O_3 concentration experienced a dramatic daytime buildup (about 50 ppbv higher than pre-/post-episode days), suggesting very strong in-situ photochemical production. For O_3 precursors and $PM_{2.5}$, their diurnal cycles in either episode days or non-episode days all show a morning peak (Fig. 5d–f) and an afternoon valley. These patterns are mainly related to the evolution of the boundary layer (PBL) since there are only few local sources in this region. The morning peaks could be related to a nighttime accumulation of primary pollutants within the nocturnal PBL, and the concentrations dropped gradually as the daytime PBL developed after sunrise. As SO_2 is mainly emitted from elevated sources like power plants, it shows a delayed peak around 10:00 LT, i.e. a time with PBL mixing height well-developed, suggesting a possible fumigation of residual layer pollution. A similar phenomenon of SO_2 has also been reported at Lin'an and Beijing (Wang et al., 2004, 2006). Comparison of the diurnal patterns of these trace gases and $PM_{2.5}$ for episode and non-episode days also shows higher concentrations of O_3 precursors, $PM_{2.5}$ and SO_2 on episode days, particularly in the early morning, suggesting an important contribution of in-situ photochemical production in a mixed plume. Another interesting point is that aerosols are generally considered as a constrain factor to O_3 production as they can affect actinic flux of UV radiation (Dickerson et al., 1997), but here we cannot see such kind of effect as $PM_{2.5}$ was also well-correlated with O_3 precursors.

ACPD
13, 2835–2876, 2013

Similar to Fig. 5, Fig. 6 gives statistical information of diurnal variations of $PM_{2.5}$, CO, SO_2, NO_y, NO, and O_3 for the days of $PM_{2.5}$ exceedances (40 % of the year) and non-exceedance days. $PM_{2.5}$ in the episode days shows dramatically higher concentrations and stronger diurnal variability than in the non-episode days, while the trace gases show similar diurnal patterns but about 20–40 % higher concentrations during episode days. The higher difference of $PM_{2.5}$ in early morning of the episode days might be related to primarily emitted sources, which could be higher in dry cold seasons because of higher emission rate and lower nocturnal PBL height. On the other hand, since the non-episode days were mainly in warm seasons, a relatively higher soil humidity and consequently much denser foliage of the plants could also cause a higher deposition rate, resulting in less accumulation of primary aerosols in the boundary layer. The missing of the afternoon valley of $PM_{2.5}$ for non-episode days might be due to the formation of secondary aerosols as that discussed in Sect. 3.2. The O_3 diurnal patterns given in Fig. 6 show higher O_3 levels for the entire period of non-episode days, which indicates favorable conditions for the formation of secondary particles (Herrmann et al., 2013). In fact, from the SO_2 diurnal pattern of non-episode days, a notable drop of SO_2 concentration associated with the O_3 peak may also indicate such kind of increased conversion.

3.3.2 Case studies for high O_3 and $PM_{2.5}$ episodes

To further understand the main causes, including weather and transport characteristics etc., of high O_3 and $PM_{2.5}$ episodes, four typical episodes were selected for detailed case studies and are presented below.

- Case I: mixed high O_3/$PM_{2.5}$ related to anticyclones: Fig. 7a presents a case of high O_3 and $PM_{2.5}$ episode occurred during 7–10 October 2011. It shows that high O_3 (up to 140 ppbv) occurred on 7 October and broad ozone peaks (up to 90 ppbv) appeared in the following two days. $PM_{2.5}$ and primary pollutants (SO_2, CO and NO_y) also reached very high levels on 7 October. Examining

ACPD
13, 2835–2876, 2013

weather-charts during the period suggests that a stagnant high pressure system dominated the Central and East China for a few days with its center located over the YRD on 7 October (see Fig. 7b). The averaged 7-day backward retroplume for the period of 7–9 October clearly shows a clockwise anticyclone flow and a long residence time over the YRD region, especially over the city clusters along the Shanghai-Nanjing axis corresponding to Fig. 1c. For the first day of the episode (7 October), the highest O_3 together with high $PM_{2.5}$ and primary pollutants CO, SO_2 and NO_y suggests a strong in-situ photochemical production in mixed regional plumes under the influence of anticyclones. In the following two days, continuous maritime air from the East China Sea and the Northwest Pacific in the east, which brought relatively fresh emission from the YRD region, also produced high O_3 concentration up to 90 ppbv. $PM_{2.5}$ mass concentration remained high with values over 100 $\mu g\,m^{-3}$ while CO, NO_y and SO_2 concentrations were moderate. In this case, the anticyclones (i.e. high pressure) caused favoring conditions, e.g. sunny weather and low wind velocities, to pollution accumulation and O_3 production. A similar relationship between high pressure and O_3 episodes has been reported elsewhere (e.g. Luo et al., 2000; Hegarty et al., 2007; Guo et al., 2009). These results clearly demonstrate a case of sub-regional transport of primary and secondary air pollutants within the YRD region under the influence of anticyclones.

– Case II: high $PM_{2.5}$ before the passage of a cold front: At the end of November 2011, an extremely high $PM_{2.5}$ episode was observed at the site, with $PM_{2.5}$ mass concentration raised over 500 $\mu g\,m^{-3}$ (Fig. 8a). Weather charts show that this case occurred under calm conditions before the passage of a strong cold front, which was at the front of a strong continental high pressure system originating from Mongolia and sweeping over Nanjing in the early morning of 30 November (see Fig. 8b). On 28 November, weak easterly and southeasterly winds dominated the YRD region, which brought pollutants from the city clusters to the site (see the high retroplume given in Fig. 8c). In contrast to Case I with the

ACPD
13, 2835–2876, 2013

influence of dominant anticyclones, no high O_3 concentrations were observed in this case which may be due to the strong titration effect of high NO (see Fig. 8a) and weak solar radiation. It is also worthwhile to point out that most of the species show a significant drop but O_3 rose to about 20 ppbv after the passage of the cold front on 30 November. Wind data suggest a strong northeast flow passing over the Yellow Sea from the north, with air masses representing the continental background from high latitudes. This phenomenon is quite different from that observed in South China, where cold fronts generally brought polluted continental outflows from East China and caused a sharp increase of primary plumes during and after the passage of the cold front (Wang et al., 2003). Besides the effect of transport, this case also shows the effect of wet deposition on some pollutants. For example, a significant drop of $PM_{2.5}$ (to as low as 10 $\mu g\,m^{-3}$) and SO_2 seems to be associated with precipitation after the passage of the cold front (see Fig. 8a).

– Case III: high $PM_{2.5}$ and O_3 related to biomass burning. As we mentioned in the introduction part, East China is the most important agricultural base in China with rice and wheat production alternating in cold and warm seasons. In the last decades, burning of crop straw has been intensive during the harvest period. Ding et al. (2013b) reported an outstanding case observed in mid-June 2012 at the SORPES site and found that episodes of extremely high $PM_{2.5}$ concentrations could substantially modify the weather. Here we make additional discussions on air pollution transport for this case. The time series given in Fig. 9a shows extremely high $PM_{2.5}$ mass concentrations observed during 9–10 June and a multi-day episode of high O_3 occurring during the following days. By using chemical components of $PM_{2.5}$, Ding et al. (2013b) clearly demonstrated that the high $PM_{2.5}$ air masses were caused by straw burning plumes mixed with fossil fuel combustion pollutants. Figure 9d further confirms the transport pathway of such kind of episode and also clearly shows that the observed air masses were associated with long residence time over the burning area and polluted region around Nanjing. On that day a low pressure located in the west of Nanjing.

ACPD
13, 2835–2876, 2013

Because of high NO concentrations and low solar radiation as a consequence of extremely high $PM_{2.5}$ concentrations, O_3 concentrations dropped to almost zero. However, two days after the episode, O_3 increased to values over 120 ppbv during 12–14 June. Again, the synoptic weather shows an anticyclone located over the YRD, and the averaged retroplume and trajectories clearly indicate that the high O_3 concentrations were associated with aged biomass burning plumes mixed with anthropogenic pollutants in the south part of YRD after being re-circulated back from the sea east of the YRD.

– Case IV: multi-day episode of high O_3 and secondary $PM_{2.5}$. This case shows a multi-day episode of O_3 and $PM_{2.5}$ observed during 15–25 July 2012. Figure 10a shows that O_3 concentrations experienced very strong diurnal cycles within these ten days, with daytime maximum O_3 concentrations over 120 ppbv on 16, 19, and 20 July. Examination of day-by-day weather charts suggests that the evolution of O_3 concentrations was closely related to the change of synoptic weather. On 16 July, a front extended from Southeast China to South Korea, with North and East China being dominated by high pressure. Under such conditions, air masses recorded at the site show clear contributions from the city clusters in the YRD region. On that day, a tropical depression (TD) was forming in the West Pacific Ocean (see Fig. 10b). The TD further developed into a typhoon (No.7, Typhoon Khanun) and its center moved to a location a few hundred kilometers southeast of the YRD on 18 July (Fig. 10c). The typhoon circulation caused a strong anti-clockwise transport of air masses from the ocean (see Fig. 10f), causing a decrease of O_3, $PM_{2.5}$, and primary pollutants on that day. However, in the following two days, a subtropical Pacific High dominated the West Pacific Ocean and East China as the typhoon weakened and disappeared after landing in Korea. Under such conditions, the air masses recorded at the site mainly came from Southeast China and swept again over the most polluted YRD city clusters in the southeast. After this episode, strong southeasterly maritime air continuously controlled East China, and daily maximum O_3 remained at high levels even with fairly

ACPD
13, 2835–2876, 2013

low concentrations of precursors, suggesting high photochemical production efficiency of O_3 in this region in summer. In this case, $PM_{2.5}$ on 16 and 20 July also showed strong evidence of secondary aerosol formation. During the two days, $PM_{2.5}$ mass concentration showed very good correlation with O_3 but not with primary pollutants CO, NO_y and SO_2. But SO_2 was generally at relatively high levels during these two days. As mentioned above, SO_2 can be easily converted to $PM_{2.5}$ sulfate in an environment of high concentration of oxidants and high air temperature. Besides oxidation of SO_2, the formation of secondary aerosols may also include contributions from biogenic emissions (VOC) because of high biomass production this region in summer, especially in the South part of the YRD.

3.4 Cross-boundary transport and implications for air pollution measures

The above results have shown an important role of sub-regional transport, especially the emissions from the YRD, on O_3 and $PM_{2.5}$ pollution in the study region. To get a more holistic understanding about the regional transport, we further carried out calculations of potential source contribution (PSC) of CO, an important O_3 precursor and tracer of combustions sources, and $PM_{2.5}$ for the measurements based on the Lagrangian dispersion simulations and an emission inventory of anthropogenic pollutants (Zhang et al., 2009). Figure 11 gives the maps of averaged PSC of CO for all the 15 episode days and the 20 pre-/post-episode days. The super-regional distributions of PSC of CO for episode and non-episode days show quite small difference (Fig. 11a and b), with high contributions from the eastern part of China, particularly the YRD region. But the zoomed view of the PSC maps for the YRD suggests completely different transport patterns. For O_3 episode days, the middle-YRD, i.e. the area along the Nanjing and Shanghai axis with its city clusters, are the main potential source regions, but non-episode days show a distinct pattern with main source regions in the North YRD and only rarely from the middle-YRD cities. These results clearly demonstrate that the middle-YRD city cluster is the major source region for high O_3 pollutions in upwind Nanjing. It needs to be mentioned that Ran et al. (2012) suggested that in the YRD

ACPD
13, 2835–2876, 2013

megacity Shanghai, the O_3 pollution mainly appeared on the urban scale, but here in the western YRD region our results clearly show an important impact of regional photochemical pollution.

Figure 12 presents the same calculations for $PM_{2.5}$ exceedances and non-exceedances days. A comparison of Fig. 12a and b shows large differences in PSC on the super-regional scale. During episode days, sources have been identified to be located on the North China Plain and generally more inland areas, while for non-episode days, the main source regions form a band covering the eastern part of China, from South China to North China, suggesting an important role of long-range transport on $PM_{2.5}$ pollution in Nanjing. The zoomed PSC maps show similar patterns but with obviously lower contributions for non-episode days, and a strong impact from the middle-YRD and North YRD. Both Fig. 12c and d show fairly high contributions of sources in the region about 20–60 km northeast to the site, which belongs to Zhenjiang City with relatively high PM emissions. It should be pointed out that the PSC of $PM_{2.5}$ only give a "rough" estimation of the potential source region from direct emitted $PM_{2.5}$, since the formation of secondary aerosols and removal processes like deposition have not be included. But nevertheless, this analysis does provide some consistent and valuable insights into cross-boundary transport in the YRD region.

To further gain quantitative understanding of cross-boundary sub-regional transport, in Table 3 we give statistics of regional contributions of CO and $PM_{2.5}$ for the entire YRD and middle-YRD regions. For the 1-yr average, emissions from the YRD and middle-YRD account for 72 % and 60 % of CO, 69 % and 53 % of $PM_{2.5}$ to the site, respectively. For O_3 episode days, the YRD, especially the middle-YRD, shows a much higher contribution than non-episode days. For $PM_{2.5}$, though the relative contributions from YRD and middle-YRD regions were of a high proportion, they was much more influence from the YRD on episode days. These results suggest a substantial contribution of sub-regional/cross-boundary transport on air quality at the site. However, currently in China environmental measures are implemented relatively independently by local governments. For the YRD region, composed of over ten cities belonging to

ACPD
13, 2835–2876, 2013

two provinces, Jiangsu and Zhejiang, and the municipality of Shanghai, it is a challenge for policy makers to establish collaborative control measures across administrative borders. Nevertheless, this is a critically important and urgent task to improve air quality in the inland downwind cities in the YRD (and beyond), such as Nanjing.

4 Summery

In this study we present an overview of 1-yr measurements of O_3 and $PM_{2.5}$ as well as related precursors at the regional background station SORPES in Nanjing, an inland YRD city in Eastern China. The characteristics and causes of O_3 and $PM_{2.5}$ concentrations are discussed by investigations of temporal variations, inter-species correlations, and case studies based on weather data and Lagrangian dispersion modeling. The main findings and conclusions can be summarized as follows:

1. Both O_3 and $PM_{2.5}$ had distinguished seasonal variations. O_3 showed a maximum in July and a secondary one in September, while $PM_{2.5}$ reached maximum values in November and a minimum in July. Within the 1-yr measurement period, there were 15 days of O_3 exceedances and 148 days (40 %) of $PM_{2.5}$ exceedances of the Ambient Air Quality Standard in China at the site, suggesting heavy air pollution in this region.

2. Correlation analysis shows a positive O_3-NO_y correlation for air masses with high air temperature in summer but a negative one in winter, and also shows a significant conversion or deposition of SO_2 under humid conditions. CO-NO_y-O_3 correlations indicated a VOC-limited regime for photochemical production of O_3 in this region, and $PM_{2.5}$-O_3 correlations clearly demonstrated substantial formation of secondary aerosols under conditions of high O_3 in summer.

3. Case studies for typical O_3 and $PM_{2.5}$ episodes suggest an important influence of air pollutants emitted from the middle-YRD, i.e. the Nanjing-Shanghai axis with

ACPD
13, 2835–2876, 2013

its city clusters in between. Synoptic weather plays an important role in the development of these episodes, and O_3 episodes are generally associated with anticyclones. Emissions from agricultural burning in this region can cause a significant rise in $PM_{2.5}$ and O_3 concentrations during the harvest seasons.

4. Calculations of potential source contributions suggest that emissions from the YRD, especially the middle-YRD, contributed to a majority of the CO (over 60 % in average) at the site. For $PM_{2.5}$, the emissions from the northern part of the YRD, mainly nearby Zhenjiang city, and the entire North China Plain are the main contributors.

This work highlights the important environmental impact from human activities in the YRD region, and suggests that collaborative control measures among different administrative regions are urgently needed to improve air quality in the west part of YRD region.

Acknowledgements. The analysis of this study was supported by National Basic Research Project (973 Project 2010CB428503) and National Natural Science Foundation of China (D0512/41075010). Part of the activities was also supported by the Academy of Finland projects (1118615, 139656) and the European Commission via ERC Advanced Grant ATM-NUCLE. The SORPES station was funded by 985 Fund and Basic Research Funds from Central Universties of Ministry of Education. The authors would like to thank P. Hari at University of Helsinki and iLEAPS SSCs for their advisory on developing the SORPES station, and thank T. Wang at The Hong Kong Polytechnic University and W. Wang at Shangdong University for their support for the measurements and for suggestions on the data analysis.

References

Allen, R. J., Sherwood, S. C., Norris, J. R., and Zender, C. S.: Recent Northern Hemisphere tropical expansion primarily driven by black carbon and tropospheric ozone, Nature, 485, doi:10.1038/nature11097, 350–353, 2012.

ACPD
13, 2835–2876, 2013

Atkinson, R.: Atmospheric chemistry of VOCs and NO_x, Atmos. Environ., 34, 2063–2101, doi:10.1016/S1352-2310(99)00460-4, 2000.

Chameides, W. L., Yu, H., Liu, S. C., Bergin, M., Zhou, X., Mearns, L., Wang., G., Kiang, C. S., Saylor, R. D., Luo, C., Huang, Y., Steiner, A., and Giorgi, F.: Case study of the effects of atmospheric aerosols and regional haze on agriculture: An opportunity to enhance crop yields in China through emission controls?, PNAS, 96, 13626–13633, 1999a.

Chameides, W. L., Li, X., Tang, X., Zhou, X., Luo, C., Kiang, C. S., John, J. St., Saylor, R. D., Liu, S. C., Lam, K. S., Wang, T., and Giorgi, F.: Is ozone pollution affecting crop yields in China, Geophys. Res. Lett., 26, 867–870, 1999b.

Cooper, O. R., Parrish, D. D., Stohl., A., Trainer, M., Nedelec, P., Thouret, V., Cammas, J. P., Oltmans, S. J., Johnson, B. J., Tarasick, D., Leblanc, T., McDermid, I. S., Jaffe, D., Gao, R., Stith,J., Ryerson, T., Aikin, K., Campos, T., Weinheimer, A., and Avery, M. A.: Increasing springtime ozone mixing ratios in the free troposphere over western North America, Nature, 463, 344–348, doi:10.1038/nature08708, 2010.

Dickerson, R. R., Kondragunta, S., Stenchikov, G. , Civerolo, K. L., Doddridge, B. G., and Holben, B. N.: The impact of aerosols on solar ultraviolet radiation and photochemical smog, Science, 278, 827–830, 1997.

Ding, A. J., Wang, T., Thouret, V., Cammas, J.-P., and Nédélec, P.: Tropospheric ozone climatology over Beijing: analysis of aircraft data from the MOZAIC program, Atmos. Chem. Phys., 8, 1–13, doi:10.5194/acp-8-1-2008, 2008.

Ding, A. J., Wang, T., Xue, L. K., Gao, J., Stohl, A., Lei, H. C., Jin, D. Z., Ren, Y., Wang, Z. F., Wei, X. L., Qi, Y. B., Liu, J., and Zhang, X. Q.: Transport of north China midlatitude cyclones: Case study of aircraft measurements in summer 2007, J. Geophys. Res., 114, D08304, doi:10.1029/2008JD011023, 2009.

Ding, A. J., Wang, T., and Fu, C. B.: Behaviors, transport characteristics and origins of CO and O_3 transported to South China: Perspectives from Lagrangian dispersion modeling, J. Geophys. Res., in review, 2013a.

Ding, A. J., Fu, C., Yang, X. Q., Sun, J. N., Petaja, T., Kerminen, V.-M., Wang, T., Xie, Y. N., Herrmann, E., Zheng, L. F., Wei, X. L., and Kulmala, M.: Intense atmospheric pollution modifies weather, in preparation, 2013b.

Draxler, R. R. and Hess, G. D.: An overview of the HYSPLIT_4 modeling system for trajectories dispersion and deposition, Aust. Meteoro. Mag., 47, 295–308, 1998.

ACPD
13, 2835–2876, 2013

Dufour, G., Eremenko, M., Orphal, J., and Flaud, J.-M.: IASI observations of seasonal and day-to-day variations of tropospheric ozone over three highly populated areas of China: Beijing, Shanghai, and Hong Kong, Atmos. Chem. Phys., 10, 3787–3801, doi:10.5194/acp-10-3787-2010, 2010.

Feng, Z. W., Jin, M. H., Zhang, F. Z., and Huang, Y. Z.: Effects of ground-level ozone (O_3) pollution on the yields of race and winter wheat in the Yangtze River Delta, J. Environ. Sci., 15, 360–362, 2003.

Fu, Q. Y., Zhuang, G. S. Wang, J., Xu, C., Huang, K., Li, J., Hou, B., Lu, T., and Streets, D. G.: Mechanism of formation of the heaviest pollution episode ever recorded in the Yangtze River Delta, China, Atmos. Environ., 42, 2023–2036, 2008.

Geng, F. H., Tie, X. X., Xu, J. M., Zhou, G. Q., Peng, L. Gao, W., Tang, X., and Zhao, C. S.: Characterizations of ozone, NOx, and VOCs measured in Shanghai, China, Atmos. Environ., 42, 6873–6883, 2008.

Guo, H., Jiang, F., Cheng, H. R., Simpson, I. J., Wang, X. M., Ding, A. J., Wang, T. J., Saunders, S. M., Wang, T., Lam, S. H. M., Blake, D. R., Zhang, Y. L., and Xie, M.: Concurrent observations of air pollutants at two sites in the Pearl River Delta and the implication of regional transport, Atmos. Chem. Phys., 9, 7343–7360, doi:10.5194/acp-9-7343-2009, 2009.

Hari, P., Andreae, M. O., Kabat, P., and Kulmala, M.: A comprehensive network of measuring stations to monitor climate change, Boreal. Eviron. Res., 14, 442–446, 2009.

Hegarty, J., Mao, H. T.,and Talbot, R.: Synoptic controls on surface ozone in the northeastern United States, J. Geophys. Res., 112, D14306, doi:10.1029/2006JD008170, 2007.

Herrmann, E., Ding, A. J., Petäjä, T., Yang, X. Q., Sun, J. N., Qi, X. M., Manninen, H., Hakala, J., Nieminen, T., Aalto, P. P., Kerminen, V.-M., Kulmala, M., and Fu, C. B.: New particle formation in the western Yangtze River Delta: first data from SORPES-station, Atmos. Chem. Phys. Discuss., 13, 1455–1488, doi:10.5194/acpd-13-1455-2013, 2013.

Huang, K., Zhuang, G., Lin, Y., Fu, J. S., Wang, Q., Liu, T., Zhang, R., Jiang, Y., Deng, C., Fu, Q., Hsu, N. C., and Cao, B.: Typical types and formation mechanisms of haze in an Eastern Asia megacity, Shanghai, Atmos. Chem. Phys., 12, 105–124, doi:10.5194/acp-12-105-2012, 2012.

Jerrett, M., Burnett, R. T., Pope III, C. A., Ito, K., Thurston, G., Krewski, D., Shi, Y. L., Calle, E., and Thun, M.: Long-term ozone exposure and mortality, New England J. Medicine, 360, 1085–1095, doi:10.1056/NEJMoa0803894, 2009.

ACPD
13, 2835–2876, 2013

Kamens, R., Jang, M., Chien, C.-J., and Leach, K.: Aerosol formation from reaction of α-pinene and ozone using a gas-phase kinetics-aerosol partitioning model, Environ. Sci. Technol., 33, 1430–1438, 1999.

Khoder, M. I.: Atmospheric conversion of sulfur dioxide to particulate sulfate and nitrogen dioxide to particulate nitrate and gaseous nitric acid in an urban area, Chemosphere, 49, 675–684, 2002.

Li, L., Chen, C. H., Fu, J. S., Huang, C., Streets, D. G., Huang, H. Y., Zhang, G. F., Wang, Y. J., Jang, C. J., Wang, H. L., Chen, Y. R., and Fu, J. M.: Air quality and emissions in the Yangtze River Delta, China, Atmos. Chem. Phys., 11, 1621–1639, doi:10.5194/acp-11-1621-2011, 2011.

Lin, W., Xu, X., Zhang, X., and Tang, J.: Contributions of pollutants from North China Plain to surface ozone at the Shangdianzi GAW Station, Atmos. Chem. Phys., 8, 5889–5898, doi:10.5194/acp-8-5889-2008, 2008.

Liu, H. Y., Jacob, D. J., Chan, L. Y., Oltmans, S. J., Bey, I., Yantosca, R. M., Harris, J. M., Duncan, B. N., and Martin, R. V.: Sources of tropospheric ozone along the Asian Pacific Rim: An analysis of ozonesonde observations, J. Geophys. Res., 107, 4573, doi:10.1029/2001JD002005, 2002.

Luo, C., St. John, J. C., Zhou, X. J., Lam, K. S., Wang, T., and Chameides, W. L.: A nonurban ozone air pollution episode over eastern China: Observation and model simulation, J. Geophys. Res., 105, 1889–1908, 2000.

Ministry of Environmental Protection of China (MEP), Ambient air quality standards (GB 3095–2012), 12 pp., China Environmental Science Press, Beijing, 2012.

Naja, M. and Akimoto, H.: Contribution of regional pollution and long-range transport to the Asia-Pacific region: Analysis of long-term ozonesonde data over Japan, J. Geophys. Res., 109, D21306, doi:10.1029/2004JD004687, 2004.

Ran, L., Zhao, C. S., Xu, W. Y., Han, M., Lu, X. Q., Han, S. Q., Lin, W. L., Xu, X. B., Gao, W., Yu, Q., Geng, F. H., Ma, N., Deng, Z. Z., and Chen, J.: Ozone production in summer in the megacities of Tianjin and Shanghai, China: a comparative study, Atmos. Chem. Phys., 12, 7531–7542, doi:10.5194/acp-12-7531-2012, 2012.

Ravishankara, A. R.: Heterogeneous and multiphase chemistry in the troposphere, Science, 276, 1058–1065, 1997.

ACPD
13, 2835–2876, 2013

Richter, A., Burrows, J. P., Nub, H., Granier, C., and Niemeier, C.: Increase in tropospheric nitrogen dioxide over China observed from space, Nature, 437, 129–132, doi:10.1038/nature04092, 2005.

Stohl, A., Forster, C., Eckhardt, S., Spichtinger, N., Huntrieser, H., Heland, J., Schlager, H., Wilhelm, S., Arnold, F., and Cooper, O.: A backward modeling study of intercontinental pollution transport using aircraft measurements, J. Geophys. Res., 108, 4370, doi:10.1029/2002JD002862, 2003.

Tie, X. X., and Cao, J. J.: Aerosol pollution in China: Present and future impact on environment, Particuology, 7, 426–431, 2009.

Tu, J., Xia, Z. G., Wang, H. S., and Li, W. Q.: Temporal variations in surface ozone and its precursors and meteorological effects at an urban site in China, Atmos. Res., 85, 310–337, 2007.

van Donkelaar, A., Martin, R. V., Brauer, M., Kahn, R., Levy, R., Verduzco, C., and Villeneuve, P. J.: Global estimates of ambient fine particulate matter concentrations from satellite-based aerosol optical depth: development and application, Environ. Health Perspectives, 118, 847–855, 2010.

Wang, G. H., Huang, L. M., Gao, S. X., Gao, S. T., and Wang, L. S.: Characterization of water-soluble species of PM10 and $PM_{2.5}$ aerosols in urban area in Nanjing, China, Atmos. Environ., 36, 1299–1307, 2002.

Wang, G. H., Kawamura, K., Xie, M. J. Hu, S. Y., Cao, J. J., An, Z. S., Waston, J., and Chow, J. C.: Organic molecular compositions and size distributions of Chinese summer and autumn aerosols from Nanjing: Characteristic haze event caused by wheat straw burning, Environ. Sci. Technol., 43, 6493–6499, 2009.

Wang, T., V. T. F. Cheung, M. Anson, and Li, Y. S.: Ozone and related gaseous pollutants in the boundary layer of eastern China: Overview of the recent measurements at a rural site, Geophys. Res. Lett., 28, 2373–2376, 2001.

Wang, T., Ding, A. J., Blake, D. R., Zahoroski, W., Poon, C. N., and Li, Y. S.: Chemical characterization of the boundary layer outflow of air pollution to Hong Kong during February–April 2001, J. Geophys. Res., 108, 8787–8801, doi:10.1029/2002JD003272, 2003.

Wang, T., Wong, C. H., Cheung, T. F., Blake, D. R., Arimoto, R., Baumann, K., Tang, J., Ding, G. A., Yu, X. M., Li, Y. S., Streets, D. G., and Simpson, I. J.: Relationships of trace gases and aerosols and the emission characteristics at Lin'an, a rural site in eastern China, during spring 2001, J. Geophys., Res., 109, D19S05, doi:10.1029/2003JD004119, 2004.

ACPD
13, 2835–2876, 2013

Ozone and fine particle in the western Yangtze River Delta

A. J. Ding et al.

Wang, T., Ding, A. J., Gao, J., and Wu, W. S.: Strong ozone production in urban plumes from Beijing, China, Geophys. Res. Lett., 33, L21806, doi:10.1029/2006GL027689, 2006.
Wang, T., Wei, X. L., Ding, A. J., Poon, C. N., Lam, K. S., Li, Y. S., Chan, L. Y., and Anson, M.: Increasing surface ozone concentrations in the background atmosphere of Southern China, 1994–2007, Atmos. Chem. Phys., 9, 6217–6227, doi:10.5194/acp-9-6217-2009, 2009.
Wang, T., Nie, W., Gao, J., Xue, L. K., Gao, X. M., Wang, X. F., Qiu, J., Poon, C. N., Meinardi, S., Blake, D., Wang, S. L., Ding, A. J., Chai, F. H., Zhang, Q. Z., and Wang, W. X.: Air quality during the 2008 Beijing Olympics: secondary pollutants and regional impact, Atmos. Chem. Phys., 10, 7603–7615, doi:10.5194/acp-10-7603-2010, 2010.
Wang, Y., Zhuang, G. S., Zhang, X. Y., Huang, K., Xu, Chang, Tang, A. H., Chen, J. M., and An, Z. S.: The ion chemistry, seasonal cycle, and sources of $PM_{2.5}$ and TSP aerosol in Shanghai, Atmos. Environ., 40, 2935–2952, 2006.
Wang, Y., Hao, J., McElroy, M. B., Munger, J. W., Ma, H., Chen, D., and Nielsen, C. P.: Ozone air quality during the 2008 Beijing Olympics: effectiveness of emission restrictions, Atmos. Chem. Phys., 9, 5237–5251, doi:10.5194/acp-9-5237-2009, 2009.
Xu, X., Lin, W., Wang, T., Yan, P., Tang, J., Meng, Z., and Wang, Y.: Long-term trend of surface ozone at a regional background station in eastern China 1991–2006: enhanced variability, Atmos. Chem. Phys., 8, 2595–2607, doi:10.5194/acp-8-2595-2008, 2008.
Yang, H. ,Yu, J. Z., Ho, S. S. H, Xu, J. H. Wu, W. S., Wan, C. H., Wang, X. D., Wang, X. R., and Wang, L. S.: The chemical composition of inorganic and carbonaceous materials in $PM_{2.5}$ in Nanjing, China, Atmos. Environ., 39, 3735–3749, 2005.
Ye, X. N., Ma, Z., Zhang, J. C., Du, H. H., Chen, J. M., Chen, H. Yang, X., Gao, W., and Geng, F. H.: Important role of ammonia on haze formation in Shanghai, Environ. Res. Lett., 6, 024019, doi:10.1088/1748-9326/6/2/024019, 2011.
Zhang, L. M., Gong, S. L., Padro, J., and Barrie, L.: A size-segregated particle dry deposition scheme for an atmospheric aerosol module, Atmos. Environ., 35, 549–560, 2001.
Zhang, M., Chen, J. M., Chen, X. Y., Cheng, T. T., Zhang, Y. L., Zhang, H. F., Ding, A. J., Wang, M., and Mellouki, A.: Urban aerosol characteristics during the World Expo 2010 in Shanghai, Aerosol. Air Quality Res., 13, 36–48, doi:10.4209/aaqr.2012.02.0024, 2013.
Zhang, Y. H., Hu, M., Zhong, L. J., Wiedensohler, A., Liu, S. C., Andreae, M. O., Wang, W., and Fan, S. J.: Regional integrated experiments on air quality over Pearl River Delta 2004 (PRIDE-PRD2004): Overview, Atmos. Environ., 42, 6157–6173, 2008.

ACPD
13, 2835–2876, 2013

Zhang, R. J., Xu, Y. F., and Han, Z. W.: Inorganic chemical composition and source signature of $PM_{2.5}$ in Beijing during ACE-Asia period, Chinese Sci. Bull., 48, 10, 1002–1005, 2003.
Zhang, Q., Streets, D. G., Carmichael, G. R., He, K. B., Huo, H., Kannari, A., Klimont, Z., Park, I. S., Reddy, S., Fu, J. S., Chen, D., Duan, L., Lei, Y., Wang, L. T., and Yao, Z. L.: Asian emissions in 2006 for the NASA INTEX-B mission, Atmos. Chem. Phys., 9, 5131–5153, doi:10.5194/acp-9-5131-2009, 2009.
Zhou, X. H., Gao, J., Wang, T., Wu, W. S., and Wang, W. X.: Measurement of black carbon aerosols near two Chinese megacities and the implications for improving emission inventories, Atmos. Environ., 43, 3918–3924, 2009.

ACPD
13, 2835–2876, 2013

Table 1. Statistics of general meteorological parameters at Nanjing for the 1-yr period August 2011–July 2012.

Month	Pressure (hPa)	Temp (°C)	RH (%)	Rainfall (mm)
Jan	1023.7	2.9	66.1	22.6
Feb	1021.1	3.0	67.5	77.0
Mar	1016.9	9.0	67.4	83.4
Apr	1007.9	18.0	64.6	60.2
May	1006.3	21.9	65.8	62.6
Jun	1000.0	25.5	68.9	20.4
Jul	999.4	29.4	67.4	184.0
Aug	1002.3	27.0	80.2	291.1
Sep	1009.4	23.1	71.0	13.1
Oct	1016.6	17.5	69.1	29.4
Nov	1018.3	14.7	72.5	23.2
Dec	1025.9	4.2	64.8	17.0

ACPD
13, 2835–2876, 2013

Table 2. Monthly statistics of average, maximum and number of exceedances of O_3 and $PM_{2.5}$ compared with the Ambient Air Quality Standards in China.

	O_3 (mg m^{-3})			$PM_{2.5}$ (μg m^{-3})		
Month	Mean	Max[1]	N.o.E.[2]	Mean	Max[1]	N.o.E.[2]
Jan	31.9	111.1	0	86.8	278.0	19
Feb	30.4	78.4	0	68.4	276.8	12
Mar	33.5	221.8	1	92.0	301.0	18
Apr	42.8	189.6	2	66.1	322.3	8
May	40.0	167.6	0	58.0	198.7	6
Jun	53.1	267.9	3	79.7	425.6	13
Jul	61.3	236.7	3	38.0	115.8	1
Aug	46.4	223.1	2	54.3	177.1	3
Sep	57.2	213.2	2	67.9	226.5	10
Oct	44.7	259.9	2	86.4	425.0	17
Nov	14.6	105.4	0	111.0	558.3	21
Dec	16.9	62.8	0	98.2	391.8	20
Annual	39.4	267.9	15	75.6	558.3	148

[1]Max means a maximum of hourly concentration.

[2]N.o.E of O_3 accounts for days with 1-h or 8-h average exceed the AAQS-CN (A standard for the Class II region: 160 and 200 mg m^{-3} for 8-h and 1-h average, respectively). N.o.E. of $PM_{2.5}$ accounts for days with 24-h average over 75 μg m^{-3}.

ACPD
13, 2835–2876, 2013

Table 3. Estimation of regional contribution of CO and $PM_{2.5}$ to the SORPES site during the 1-yr period.

Region	O_3 Episode	CO (ppm) Pre-/Post-O_3 episode	Annual Rate	Episode	$PM_{2.5}$ ($\mu g\,m^{-3}$) Non-episode	Annual Rate
YRD	0.632	0.547	72.1 %	51.6	38.8	69.0 %
M_YRD	0.548	0.414	59.7 %	39.3	30.0	53.0 %

ACPD
13, 2835–2876, 2013

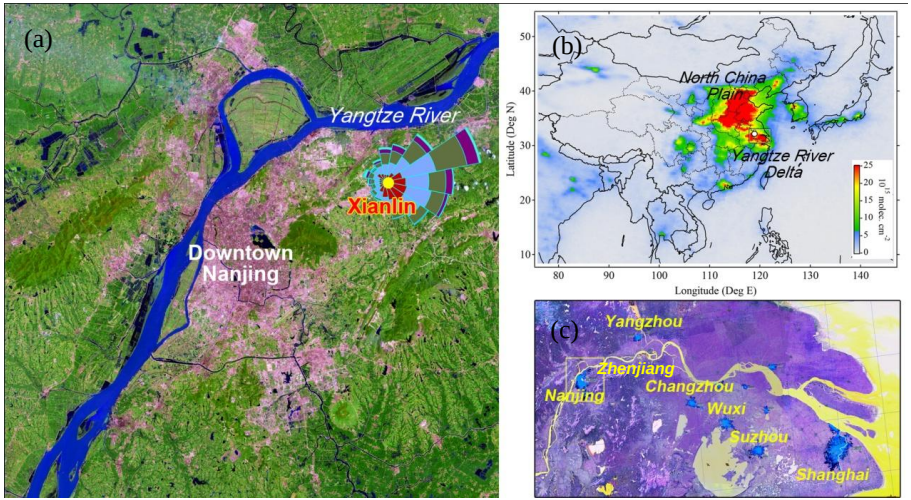

Fig. 1. (a) A map showing the location of the SORPES Xianlin site. **(b)** Averaged GOME2 tropospheric NO_2 columns for the period of August 2011-July 2012. **(c)** A map showing cities in the Yangtze River Delta. The GOME2 data were accessed from Tropospheric Emission Monitoring Internet Service of KNMI (www.temis.nl).

ACPD
13, 2835–2876, 2013

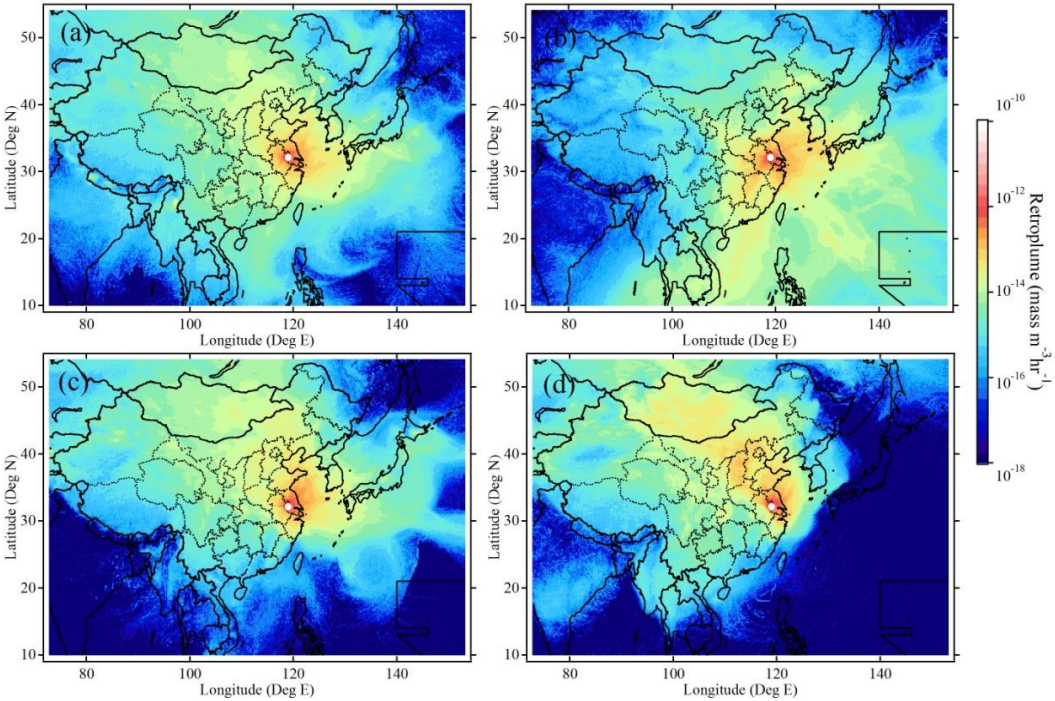

Fig. 2. Averaged retroplume ("footprint" residence time) showing transport pathways of air masses observed at Nanjing during **(a)** spring, **(b)** summer, **(c)** autumn, and **(d)** winter, respectively, during the 1-yr period.

ACPD
13, 2835–2876, 2013

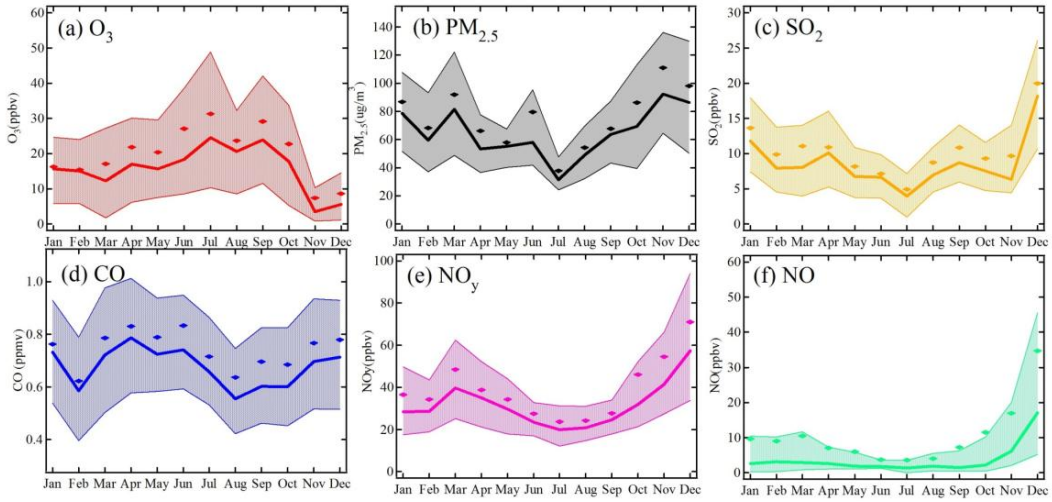

Fig. 3. Seasonal variation of **(a)** O_3, **(b)** $PM_{2.5}$, **(c)** SO_2, **(d)** CO, **(e)** NO_y and **(f)** NO. Bold solid lines are the medium values, diamonds show the monthly averages and thin solid lines represent percentiles of 75 % and 25 %.

ACPD
13, 2835–2876, 2013

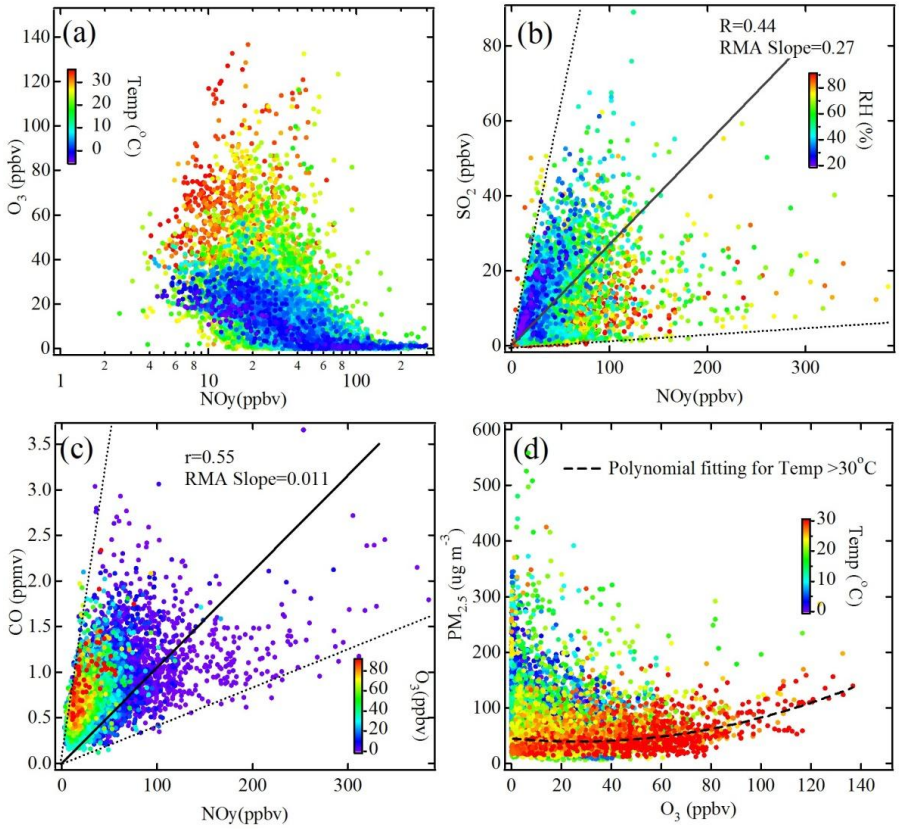

Fig. 4. Scattering plots of **(a)** O_3-NO_y color-coded with air temperature, **(b)** SO_2-NO_y color-coded with relative humidity, **(c)** CO-NO_y color-coded with O_3 concentrations, and **(d)** $PM_{2.5}$-O_3 color-coded with air temperature.

ACPD
13, 2835–2876, 2013

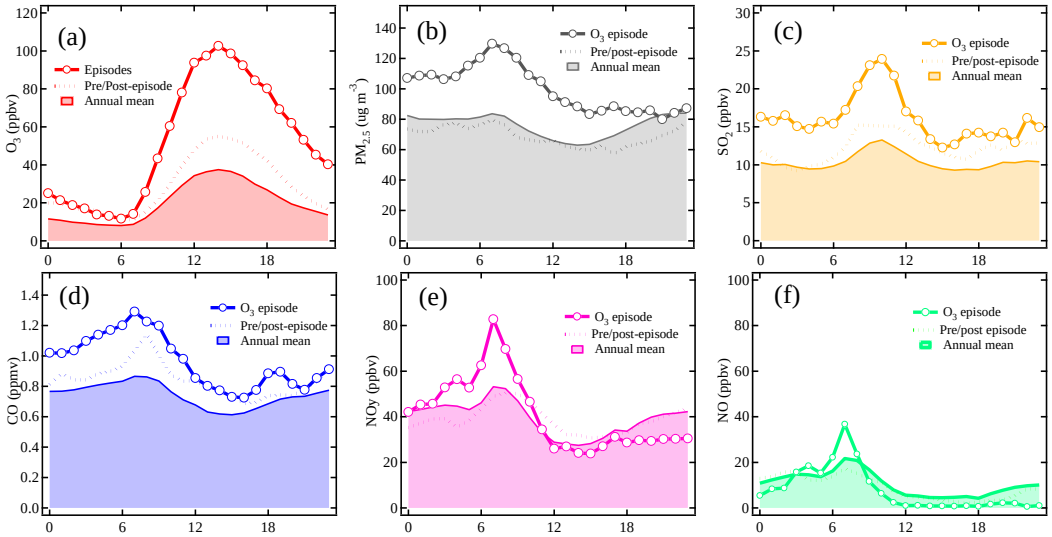

Fig. 5. Diurnal variations of **(a)** O_3, **(b)** $PM_{2.5}$, **(c)** SO_2, **(d)** CO, **(e)** NO_y, and **(f)** NO, averaged for O_3 episode days with exceedances of the AAQS-CN and the pre-/post-episode days, and the entire 1-yr period.

ACPD
13, 2835–2876, 2013

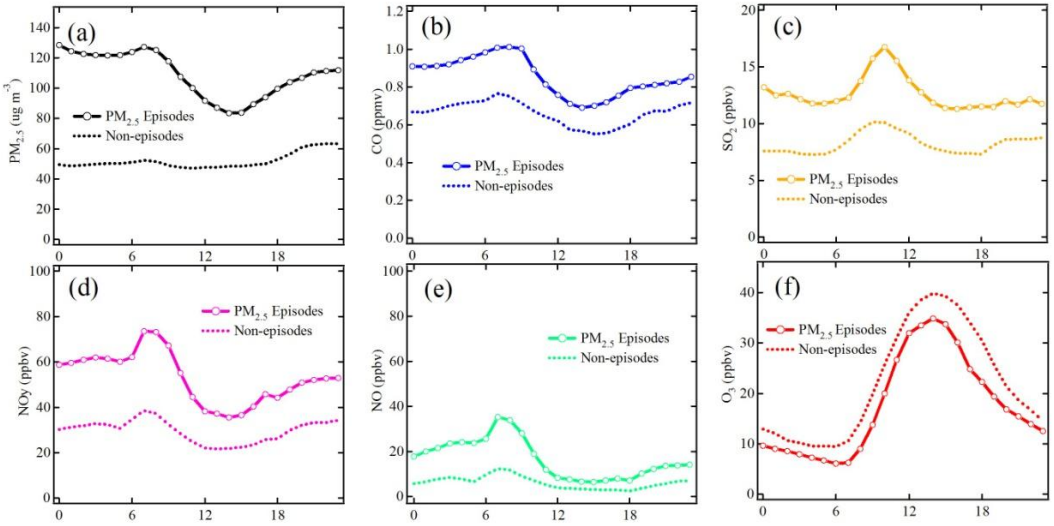

Fig. 6. Diurnal variations of **(a)** $PM_{2.5}$, **(b)** CO, **(c)** SO_2, **(d)** NO_y, **(e)** NO, and **(f)** O_3, averaged for $PM_{2.5}$ episode days with exceedances of the AAQS-CN and the non-episode days.

ACPD
13, 2835–2876, 2013

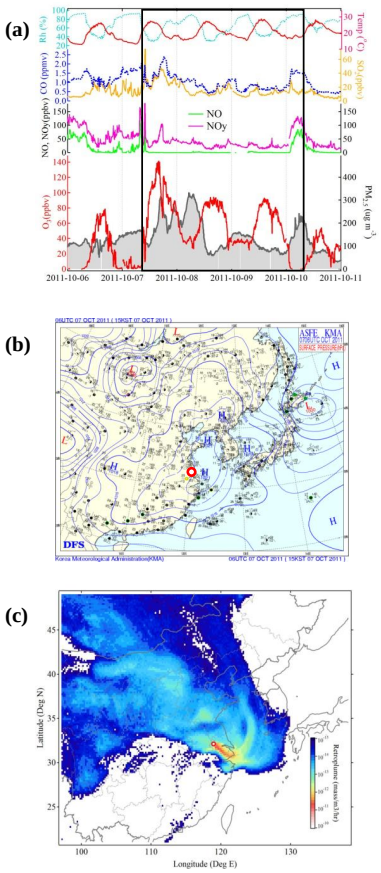

Fig. 7. (a) Time series of O_3, $PM_{2.5}$, related trace gases and meteorological parameters for Case I , i.e. 6–10 October 2011. **(b)** Weather chart on 7 October 2011. **(c)** Averaged retroplume of air masses at Nanjing for the period shown as back box shown in 7**(a)**.

ACPD
13, 2835–2876, 2013

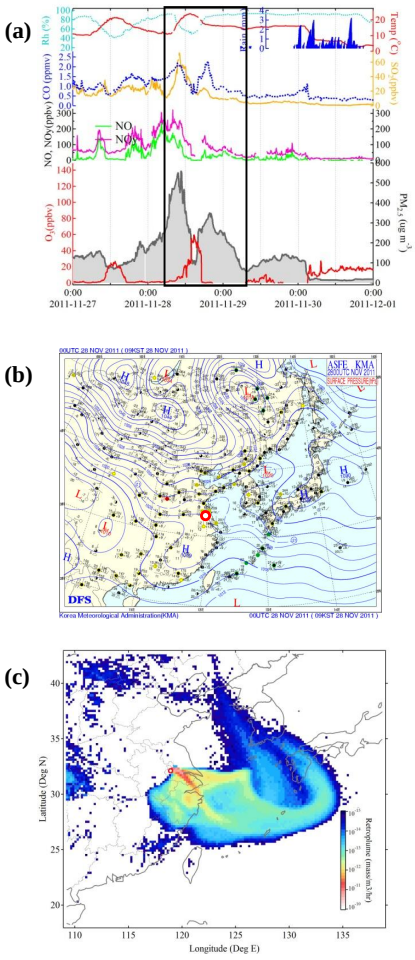

Fig. 8. Same as Fig. 7 but for Case II, i.e. 27–30 November 2011.

ACPD
13, 2835–2876, 2013

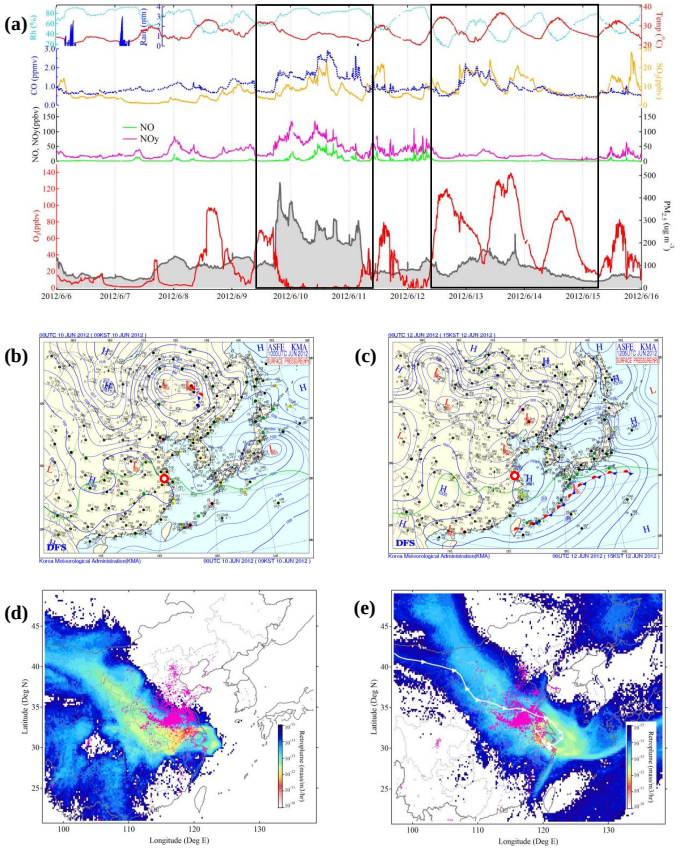

Fig. 9. (a) Time series of O_3, $PM_{2.5}$, related trace gases and meteorological parameters for Case III, i.e. 9–15 June 2012. **(b)** And **(c)** Weather charts for 10 and 12 June 2011, respectively. **(d)** And **(c)** Averaged retroplumes for the periods marked with black boxs in 9a. Pink points give MODIS fire accounts for the period of 6–13 June 2012. White line with triangles given in 9e shows 7-day backward trajectory for 15:00 LT on 13 June 2012.

ACPD
13, 2835–2876, 2013

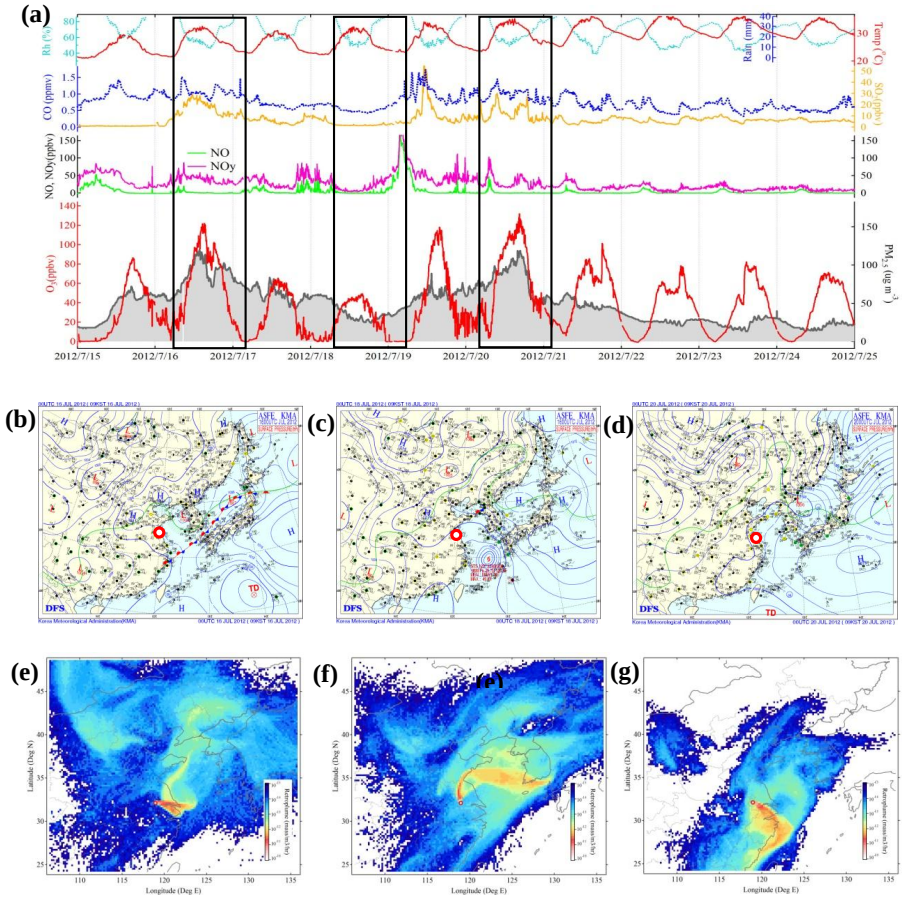

Fig. 10. (a) Same as Fig. 9a but for Case IV, i.e. 15–25 July 2012. **(b–d)** And **(e-g)** show weather charts and averaged retroplumes for the three periods marked in Fig. 10a.

ACPD
13, 2835–2876, 2013

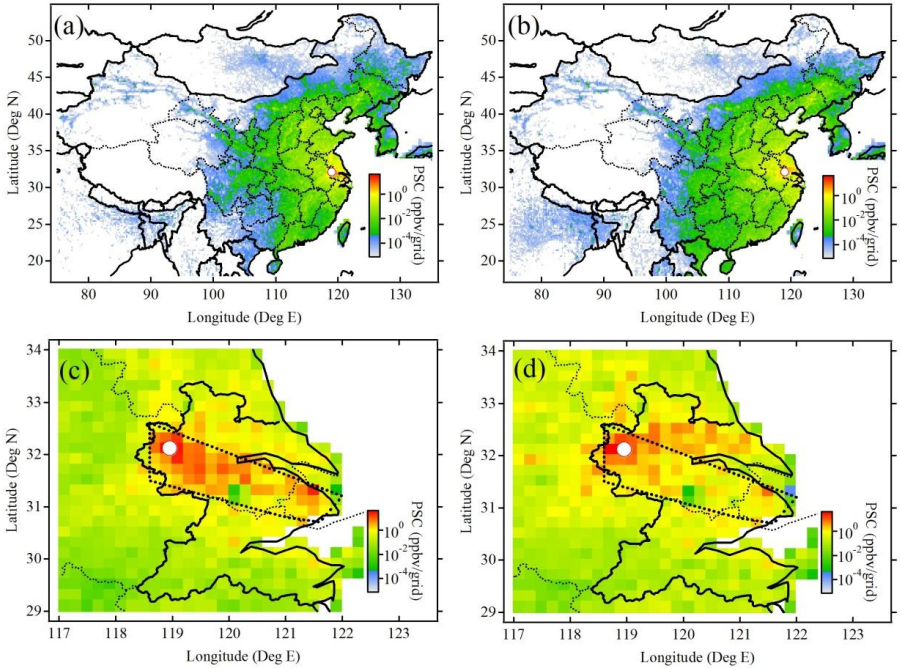

Fig. 11. (a) And **(b)** averaged distributions of potential source contribution of CO for episode days with O_3 exceedances and pre-/post- episode days, respectively. **(c)** And **(d)** a zoomed view for 11**(a)** and 11**(b)**, respectively.

ACPD
13, 2835–2876, 2013

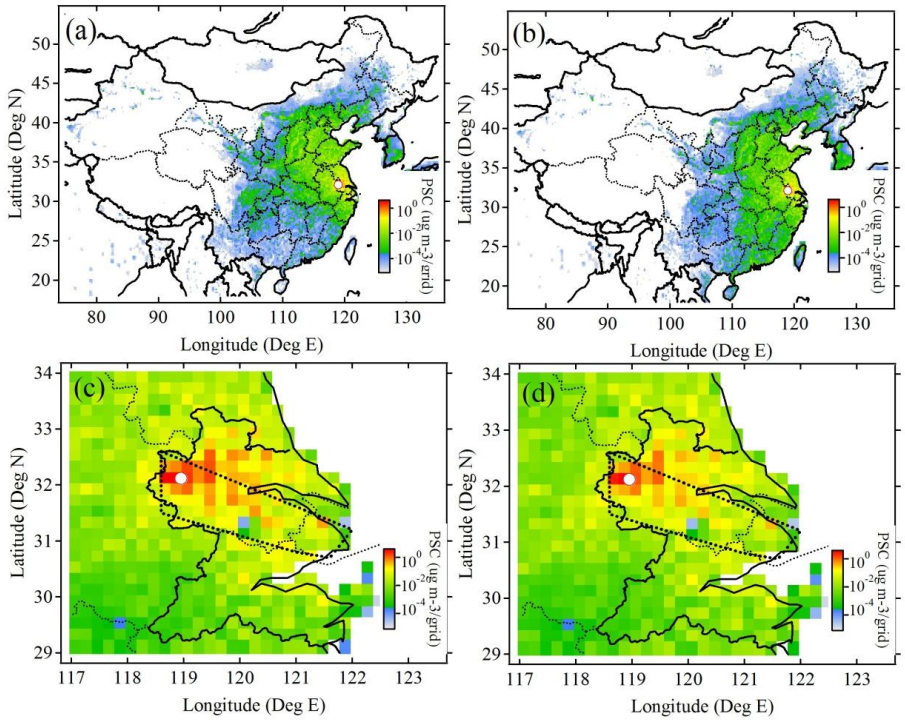

Fig. 12. Same as Fig. 11 but for days with $PM_{2.5}$ exceedances and non-episode days, respectively.

ACPD
13, 2835–2876, 2013